Bridgemill bridge bearing capacity assessment by a discrete element method

G.A.F. Rouxinol
Polytechnic Institute of Viseu — School of Technology, Department of Civil Engineering, Viseu, Portugal

P. Providência
University of Coimbra, Portugal

J.V. Lemos
LNEC, Lisbon, Portugal

ABSTRACT: The calculation of the bearing capacity of the Bridgemill masonry arch bridge is presented using the mixed discrete element method. This bridge has been the subject of several studies aiming at the calibration and validation of structural analysis numerical models. Hendry, Davies and Royles subjected the bridge to an *in situ* test, where a knife type load was applied at a quarter span until collapse. A 2D model of rigid discrete elements including blocks and particles describes accurately its limit behaviour. Four different cases are considered to analyze the bridge behaviour and estimate its load capacity, two with the isolated arch, and two combining the arch with the fill and the spandrel wall. The 3D collapse load is estimated by combination of those solutions. Due to the unavailability of several Bridgemill bridge material properties, the equivalent values measured on experimental tests for similar structures had to be selected.

1 INTRODUCTION

The main objective of this communication is to illustrate the application of a mixed discrete element method program. This program is specially adapted to the structural analysis of masonry structures made up of two types of rigid discrete elements: (i) polygonal, also referred to as blocks (b), with three to five vertices and (ii) circular, referred to as particles (p).

The structural system deformability results solely from the adopted point contact model, where the compression forces associated to contact between discrete elements produce a small superposition of their boundaries. The constitutive model associated to each contact can be formulated either in terms of stresses or forces. While in the stress formulation the influence area for each contact must be permanently updated during a pseudo-temporal analysis (but never becoming smaller than a predetermined minimum value in order to avoid severe numerical oscillations of the contact force), in the force formulation such an influence area is kept fixed. For materials with a small compressive strength some crushing phenomena may occur, requiring the use of an elastoplastic stress-strain relation, and it becomes advisable to adopt the stress formulation. However for masonry arches the voussoirs' compression strength is usually large, with a collapse mechanism exhibiting the four "plastic hinges" pattern, and thus the more efficient force formulation is ideal for the calculation of the structure's ultimate load.

2 BRIEF DESCRIPTION OF THE MIXED DISCRETE ELEMENT METHOD (MDEM)

This section presents a succinct description of the version of the discrete element method (DEM) used in the calculations. For a more detailed portrayal see Rouxinol *et al.* (2006). The mixed discrete element method follows in a general form both the DEM for blocks, Cundall (1971), and the DEM for particles, Cundall and Strack (1979). The junction of these two models

required the definition of new types of contacts and the development of sub-algorithms for detection of new contacts and updating / removal of old contacts. The sub-algorithm implemented for detection and updating follows the method proposed by Cundall (1988) and the enveloping volumes method, Williams (1988). In general terms the DEM consists in the iterative and alternate application of (i) the movement equations resulting from Newton's second law, determining the displacement of the centre of mass of each discrete element, and (ii) of a constitutive force-displacement relation at the contact level, including both normal and shear components. A quasi-static analysis requires the use of numerical damping for dissipating the system's kinetic energy, which allows to classify this method as a dynamical relaxation method. Eventually, for a finite number of iterations depending upon a selected maximum admissible error, the iteration cycle converges into either an equilibrium resting state or a collapse mode.

The numerical damping can be either (i) global when proportional to the velocity (viscous) or (ii) local when proportional to the out-of-balance forces. For stability of the explicit integration of the damped movement equations, the "time" step must be smaller than a critical value given by twice the inverse of the maximum frequency of the linearized structural system, Bathe (1982). Thus the program includes routines to solve the associated eigenvalue problem. In order to reduce the computation time required for the eigenvalue analysis of systems with large number of DOF simple approximate 1DOF methods can be used, which roughly depend on the minimum particle mass and the maximum contact stiffness, Morikawa et al. (1993).

The relative velocity at a generic contact point gives the relative displacement increment as a function of the time step. Then the contact's influence area and constitutive relation give the contact force increment, and the total contact force is updated. The normal component of this force is calculated with an elastoplastic or a linear elastic model. When this component changes from compression to traction the contact is eliminated. The shear component of the force obeys the Mohr-Coulomb strength criterion. The updated contact forces of the contacts of each element are statically reduced to its centre of mass together with other externally applied loads including those due to gravity. A new computation cycle begins, until convergence is achieved, solving the movement equations for new values for the relative velocity at the contacts, etc.

Due to the large amount of both blocks and particles that these structural systems may contain, the program includes routines which automatically, based on some geometric parameters, generate the discrete element mesh of the main structural components of a masonry bridge, like semi-circular and shallow/deep segmental arches, spandrel walls, columns and (using the expansion ratio method) the fill material. The program is capable of bidirectional communication in an AutoCAD® (DXF™) formatted context which means that (i) the referred meshes can be exported and viewed within that standard CAD software and (ii) it can import predefined meshes, obtained by photogrammetry, Valença (2006), or other techniques.

The approximated isotropic stress for each block, as given by the divergence theorem, Potyondy et al. (2004), is computed during the iteration process. For the visualisation of both stress and displacement fields the post processing includes graphic routines, which are crucial to assimilate the large amounts of output.

3   DETAILED ANALYSIS OF BRIDGEMILL MASONRY ARCH BRIDGE

In Rouxinol et al. (2006) the full description of the MDEM used in the present calculations is illustrated with a brief study of Bridgemill's masonry arch bridge collapse behaviour. Hendry, Davies and Royles, as cited by Page (1993), performed an in $situ$ test with a "knife" type load with length $L_0 = 0.750$ m , see Fig. 1, crossing the whole 8.3 m bridge width, applied at a quarter span of the arch, incremented until a maximum of 3100 kN. (This does not correspond to the effective collapse, but merely to the extensive fissuring at the collapse mechanism hinges.) The detailed DEM numerical analysis of this problem is presented next. The incremental knife load is applied to four distinct structural/loading schemes: (i) isolated masonry arch without both the fill material and the corresponding death weight; (ii) isolated masonry arch without fill material but with the corresponding death weight; (iii) masonry arch plus fill material; (iv) masonry arch plus spandrel wall. The arch mesh has 62 blocks, one for each voussoir, besides the fully fixed abutments. The ultimate (effective collapse) load is given for a nondimensional unitary width and, in parenthesis, for the real width of the bridge to compare with Hendry's results.

3.1 Geometric and mechanical properties

Page (1993) provides the geometric data and the materials' mechanical properties of the bridge. However that report lacks some crucial parameters. This entailed the selection of some values referred to in the specialized literature for similar structures along with the analysis of the influence on the results as these speculative values were varied within expectable ranges.

The $l = 18.30$ m span and $r = 2.85$ m rise at midspan bridge's parabolic arch is made up of voussoirs with an height of $h_b = 0.711$ m. The real parabola was replaced by a segmented arch was, as the difference between these curves is small due to the magnitude of the ratio l/r, Vermeltfoort (2001). The distance from the keystone extrados to the pavement surface is 0.478 m (depth of fill at crown 0.203 m, sub-base thickness 0.125 m and bituminous layer 0.150 m).

For the sandstone voussoirs and spandrel wall's bricks the deformation modulus (modulus of elasticity) is $E_b = 15$ GPa, the density is $\rho_b = 2100$ kg/m^3 and each block's compressive strength is $f_{b,1} = 43.8$ MPa.

For the fill material particles, composed of a mixture of gravel, sand and clay, the adopted deformation modulus is $E_f = 40$ GPa, Molins (1998), and the density is $\rho_f = 1890$ kg/m^3.

A first estimate of the normal and shear contact elastic stiffnesses per unit area satisfy

$$\frac{1}{k_n} = \frac{1}{k'_n} + \frac{l_{cm}}{E_b}; \quad \frac{1}{k_s} = \frac{1}{k'_s} + \frac{l_{cm}}{G_b} \tag{1}$$

Vieira (1997), where l_{cm} is the distance between the centres of mass of the two contacting blocks (measured along the contact's normal), k'_n and k'_s are the effective joint normal and shear stiffnesses per unit area and G_b is the blocks' elastic shear modulus. Table 1 gives these parameters' values for the three contacts' types. The values adopted for $k'_{,b-b}$, $k'_{,b-p}$ and the Poisson's ratio ν were experimentally determined by Costa (2002) for Lagoncinha's bridge.

Table 1 : Calculation of the contact stiffnesses k_n and k_s.

	d_{cm}	ν	E	G	k'_n	k'_s	k_n	k_s
	m	—	GPa	GPa	GPa / m	GPa / m	GPa / m	GPa / m
b-b	0.3208	0.2	15.000	6.250	5.400	0.590	4.840	0.573
b-p	0.1500	0.2	15.000	6.250	65.000	27.000	4.840	0.573
p-p	0.1500	0.2	0.040	0.017	—	—	0.532	0.222

The values used for the p-p contact stiffnesses, k_n and k_s, must be such that the overall fill's rigidity is similar to E_f. In order to calculate them the arbitrary values $k'_{,p-p} \equiv k'_{,b-p}$ were first assumed and the values of k_n and k_s specified by (1) calculated and referred to as $k_{n,(1)} = 0.266$ GPa / m and $k_{s,(1)} = 0.111$ GPa / m. Then an 1 m side square's sample was isolated from the fill's mesh, Fig. 1a, replacing, when possible, the partially truncated particles by smaller ones. Subsequently this sample was confined with three fixed blocks, placed below and on its sides, Figure 1b. A fourth block weighing 2.6 kN and free to move vertically was then subjected to load increments of 25 kN, Fig. 1c, and its vertical displacement measured, Fig. 2.

This procedure was performed for values of k_n and k_s given by one, two, four, six and eight times $k_{n,(1)}$ and $k_{s,(1)}$, while all the other parameters were kept fixed. The average tangent deformation modulus is respectively 22, 28, 34, 42 and 48 MPa and the secant deformation modulus (difference between first and last results) 16, 26, 12, 14 and 18 MPa. The three last values are significantly higher if the first four load steps are ignored, 28, 43 and 54 MPa. In order to satisfy the value specified for E_f the stiffnesses adopted for the p-p contacts should have been about $k_n = 6k_{n,(1)}$ and $k_s = 6k_{s,(1)}$ but, by an oversight, in the results presented below the values $k_n = 2k_{n,(1)} = 0.532$ GPa / m and $k_s = 2k_{s,(1)} = 0.222$ GPa / m were used, see Table 1.
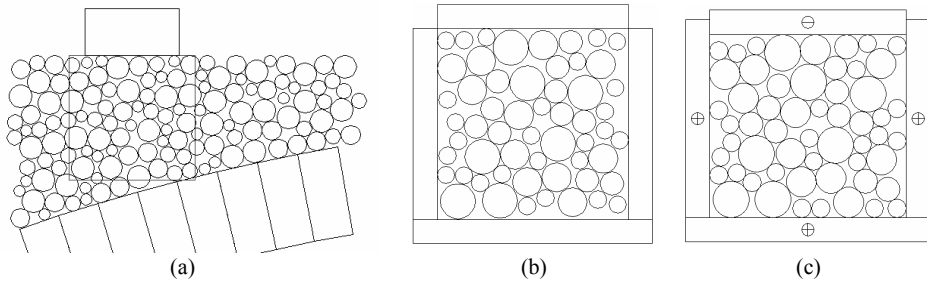
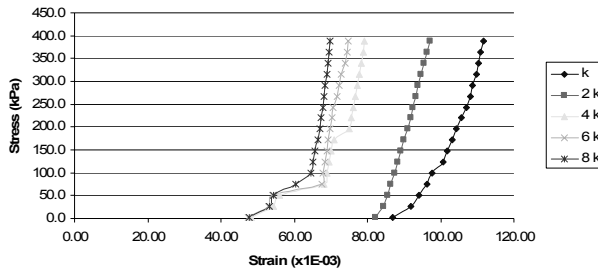Figure 1 : (a) Particle's mesh sample; (b) confinement of the sample; (c) loading of the confined sample.

Figure 2 : Stress-strain relation for the confined particles.

For the b-p contacts formulae (1) gave $k_n = 0.079 \,\mathrm{GPa/m}$ and $k_s = 0.033 \,\mathrm{GPa/m}$, but these values had to be increased ($k_{\_,b-p} \equiv k_{\_,b-b}$) in order to avoid excessive superposition.

Table 2 gives the remaining required parameters. Following Heyman (1982) and Lemos (2006) the sandstone tensile strength $f_{b,t}$ is ignored. The fill material's tensile strength $f_{f,t}$ is also ignored. Due to the lacking record of the internal friction angle φ, the value found in lab tests for the Serra do Pilar's Monastery, Portugal, Muralha (2000), was used for all types of contact.

Table 2 : Further properties for the blocks and joints.

	c kPa	ϕ °	$f_{b,t}, f_{f,t}$ MPa	$f_{b,1}$ MPa	$l_{c,\,fixed}$ m	$l_{c,\min}$ m
b-b	0	35.6	0	43.8	0.3455	0.0711
b-p	10	35.6	0	—	0.1500	—
p-p	10	35.6	0	—	0.1500	—

For an analysis per unit width, the contact's influence area is given by $a_c = l_c \times 1 = l_c$, where l_c is the contact's influence length. If l_c is allowed to vary for the b-b contacts, a minimum must be defined and the value $l_{c,\min} = h_b / 10$ was considered following Coulomb, Heyman (1995). If l_c is fixed then for the b-b contacts it is given by half the distance between the contact points along the height of the blocks, $l_{c,\,fixed} = (h_b - d_r)/2 = 0.3455 \,\mathrm{m}$ where d_r is the rounding parameter of the blocks' vertices, see Rouxinol et al. (2006) and, for the b-p and p-p contacts, by the average of the diameters of the particles and/or radius of rounded vertices.

For the p-p and b-p contacts a cohesion of $c_f = 10 \,\mathrm{kPa}$ was adopted ($c_b = 0$), as justified by the range $[1.0, 20.0] \,\mathrm{kPa}$ specified by Cavicchi et al. (2005) and Gago et al. (2003).

In the following analyses the dead weight of the discrete elements of each model are "applied" first and the other loads afterwards. The arch's abutments upper face measures 2.0 m.

3.2 Case 1 – Isolated arch with neither the fill nor its action on the arch

In this case the arch carries only its dead weight and the "knife" load F. A load dispersion angle of 26°, corresponding to a vertical to horizontal slope of $s = 2:1$, was adopted. The load degradation surface intersects the arch's extrados at the points P_1 and P_2 with depths h_1 and h_2. These points define a line segment with horizontal projection $L = L_0 + (h_1 + h_2)/s$. The load distribution between these points is approximately trapezoidal with magnitude inversely proportional to the depth, *i.e.* $q_1 = q \cdot F/h_1$ and $q_2 = q \cdot F/h_2$. Thus, by equilibrium

$$q = \frac{2}{L}\frac{h_1 h_2}{h_1 + h_2}; \quad \Rightarrow q_1 = \frac{2F}{L}\frac{h_2}{h_1 + h_2}, \quad q_2 = \frac{2F}{L}\frac{h_1}{h_1 + h_2} \tag{2}$$

First the performance of the two types of damping was evaluated: the global viscous and the local non-viscous. In the viscous case, the possibility of adapting the damping intensity during the iteration cycle, global adaptive damping, was also assessed. The response load-displacement curves (for the quarter span voussoir) are coincident, see Fig. 3a, and the collapse load is 204.82 kN / m (1700 kN). The total number of iterations for the local and the adaptive global damping cases is similar (about 120 000) and ten times smaller than for the non-adaptive global damping. Subsequently, and using the adaptive global damping, the sensibility of the response to the contact's influence length being kept fixed or left free was assessed, and it was verified that both the collapse load and mechanism were preserved, Fig. 4a. In fact it was observed a significant variation of the maximum stress value, from 1.49 to 6.06 MPa, depending on l_c being fixed or free, even though both values are below f_b.

3.3 Case 2 – Isolated arch with vertical loads simulating the fill action on the arch

In this case the fill is once more excluded from the DEM model, but its weight is considered, together with the arch's weight and, like in Case 1, the incremental knife load. Fig. 3b represents the load-displacement relation obtained, with a collapse load of 325.30 kN / m (2700 kN). The differences observed in Fig. 3b between the final displacement values, for the different types of damping, correspond to different collapse stages. The number of iterations required for the local and adaptive global damping cases was about 230 000 and for the non-adaptive global 2 350 000. The maximum compression stress is again beneath f_b for fixed (2.74 MPa) or non-fixed (10.57 MPa) contact influence length. Fig. 4b shows the collapse mechanism.

3.4 Case 3 – Combined effect of the arch and the fill simulated by particles

In this case the point load is applied to the combined system formed by arch and fill material. The radius expansion method, ITASCA (2002), is used to define the mesh of particles.

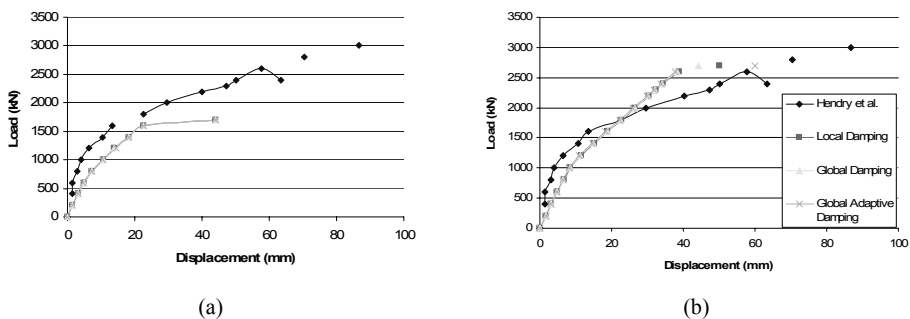(a)   (b)

Figure 3 : Load-displacement relation for (a) Case 1; (b) Case 2.
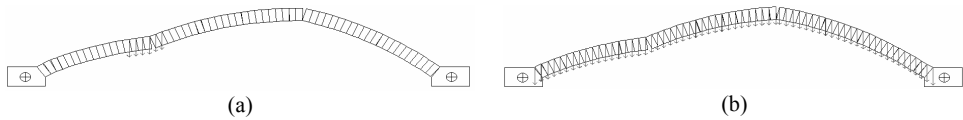
Figure 4 : Collapse mechanism for (a) Case 1; (b) Case 2. Arrows indicate the applied loads' location.
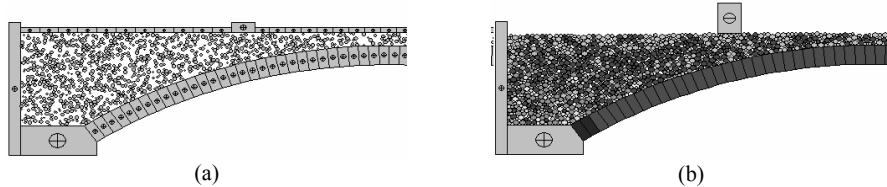

Figure 5 : Discrete element mesh (a) previous and (b) after the particles' expansion stage.

During the expansion stage the arch blocks are kept fixed. The introduction of an upper layer of fixed blocks above the pavement level accelerates the rate of convergence of this stage, Fig. 5a. After the expansion stage this layer is removed and the arch blocks set free, Fig. 5b. The fill mesh contains 1984 particles. The knife load is applied by means of an additional block weighing 17.72 kN / m (147 kN) prevented from either rotate or move horizontally.

The adaptive global damping was used while the contact influence length was kept fixed. For a point load value of 379.2 kN / m (3147 kN) the system was unable to converge (even with either the local or the non-adaptive global damping schemes), showing an oscillating and non-vanishing total out-of-balance force of 0.2–0.3 kN / m, which often occurs in the DEM when a collapse state is approached. A further increment of 12.04 kN / m (100 kN) produced the immediate collapse of the arch, corresponding to a collapse load of 391.2 kN / m (3247 kN), Fig. 8. Once more the maximum compressive stress (3.01 MPa on the next to the last load step) is under f_b . Fig. 6 illustrates the collapse mechanism, revealing the prior rupture of the fill material and the collapse of the arch for an almost direct application of the point load on the arch.

   In Rouxinol et al. (2006) the fill was modelled with only 239 particles, producing a collapse load of 2937.5 kN (353.9 kN / m), including the load carrying block weighting 37.5 kN. Thus, the refinement of the mesh allowed for an evenly stress redistribution, avoiding some localised phenomena responsible for interlocked particle clusters, both (i) between the arch's extrados and the particles and (ii) between the particles themselves. The lateral support conditions in the previous model were introduced with an inclined abutment block. In the present model, a vertical fixed block is used, but further away from the arch to avoid effects on the collapse mode.

3.5   Case 4 – Combined behaviour of arch plus brickwork spandrel wall

In this case the point load is applied to the combined system consisting of the arch and spandrel wall. The $22 \times 20 \times 30$ cm dimensions brickwork mesh considered in Rouxinol *et al*. (2006) is now replaced by the coarser $22 \times 40 \times 60$ cm . The knife load is applied on two bricks of the upper layer. Both the local and the adaptive global damping cases performed well, Fig. 8, giving a collapse load of 433.73 kN / m (3600 kN). On the contrary, the non-adaptive damping case required an excessive number of iterations. The contact influence length was kept fixed. The maximum compressive stress was bellow the admissible values for both the brickwork and voussoirs (2.83 MPa on the next to the last load step). Fig. 7 illustrates the collapse mechanism.

   An weighed average of the collapse load values for Cases 3 and 4 gives a rather rough estimative of 3265 kN for the collapse load of the bridge (for a width of the fill section of 7.86 m and of the walls of 0.44 m), corresponding to an error of +5% when compared to the value obtained *in situ*. (Note that this totally omits some 3D features which might reduce the collapse load as well as the favourable shell behaviour of the arch).
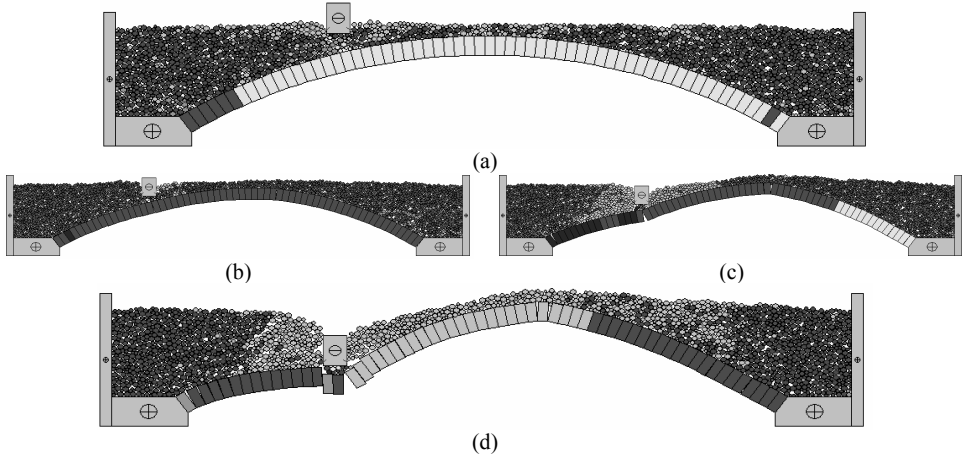
Figure 6 : Case 3 for (a) $F = 800$ kN ; (b) impending collapse; (c,d) effective collapse.

4 CONCLUSIONS

The example presented shows the potential of the mixed discrete element method (MDEM) to become an useful and dependable tool for the determination of the collapse load of masonry arch bridges. It can be concluded that the use of circular discrete elements (particles) to model the fill material gives a failure load quite close to the obtained with the *in situ* test (which appears not to correspond to the effective collapse but instead to the formation of the collapse mechanism). Case 1 with its lower value for the collapse load also confirms the relevance of including the fill material in the DEM model. It would also be expected that Case 4, which is the stiffest, would give the highest value for the collapse load. Finally, Case 2 is interesting from the practical point of view because it provides a simple way to estimate the collapse load.

The comparison of the numerical damping schemes showed that, even though they force the algorithm to converge to the same final state, the most efficient are the local or the adaptive global. Finally, the comparison between fixed and non-fixed contact influence length produced some differences at the stress field level but without consequences for the collapse state, including the possibility of collapse by material crushing.
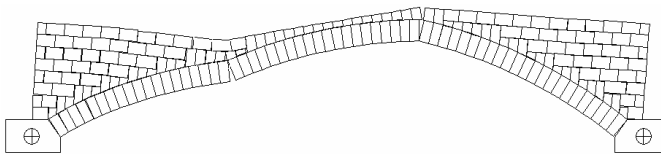

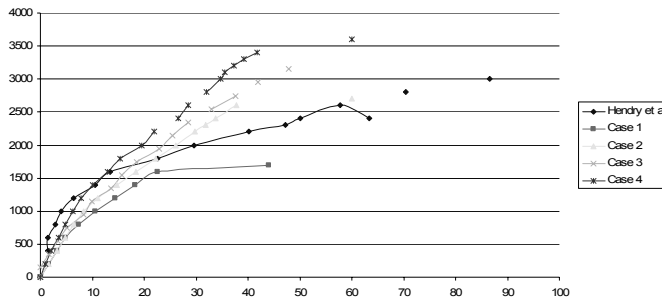Figure 7 : Collapse mechanism for Case 4.

Figure 8 : Load-displacement relations.

REFERENCES

Bathe, K.J. 1982. *Finite element procedures in engineering analysis*, Prentice-Hall.
Cavicchi, A. and Gambarotta, L. 2005. Collapse analysis of masonry bridges taking into account arch-fill interaction. *Engineering Structures* 27, p. 605-615.
Costa, C. 2002. Analysis of the behaviour of bridge of Lagoncinha under automobile traffic. M.Sc. Thesis, University of Porto, Portugal (in Portuguese)
Cundall, P.A. 1971. A Computer Model for Simulating Progressive Large Scale Movements in Blocky Rock Systems. In *Proc. Symposium Int. Society of Rock Mechanics*, vol. 1, paper II-8. Nancy, France.
Cundall, P.A. and Strack, O.D.L. 1979. A discrete numerical model for granular assemblies. *Géotechnique.* 29, n.1, p. 47-65.
Cundall, P.A. 1988. Formulation of three-dimensional distinct element model – Part I: A scheme to detect and represent contacts in a system composed of many polyhedral blocks. *Int. J. Rock Mech. Min. Sci. & Geomech. Abstr.* 25(3), p. 107-116.
Gago, S.G., Alfaiate, J. and Almeida J.R. 2003. Numerical simulation of an experimental test of a masonry bridge. In *VII Congresso de Mecânica Aplicada e Computacional*, vol. 2, p.935-944, University of Évora, Portugal (in Portuguese)
Heyman, J.M.A. 1982. *The masonry arch.* Ellis Horwood
Heyman, J.M.A. 1995. *Theory, history and conservation restoration of masonry structures*. Madrid: Instituto Juan de Herrera. (in Castilian)
ITASCA Consulting Group, Inc. 2002. *PFC2D – Particle Flow Code in 2 Dimensions. User's Guide*. Version 3.0. Minneapolis USA.
Lemos, J.V. 2006. Modeling of Historical Masonry with Discrete Elements. In C.A. Mota Soares, J.A.C. Martins, H.C. Rodrigues and J.A.C. Ambrósio (eds.), *Computational Mechanics – Solids, Structures and Coupled Problems*, p. 375-391. Springer.
Molins, C. 1998. Numerical simulation of the response of arch Bridges. In P. Roca, J.L. González, E. Oñate and P.B. Lourenço (eds.), *Structural Analysis of Historical Constructions II, Proc. Int. Seminar,* p. 93-123. Barcelona: CIMNE.
Morikawa, H. Sawamoto, Y. and Kobayashi, N. 1993. Local Fracture Analysis of a Reinforced Concrete Slab by the Discrete Element Method. In J.R Williams and G.G.W.Mustoe (eds.), *Proc. 2nd Int. Conf.on Discrete Element Methods*, p. 275-286. Boston: MIT Press.
Muralha, J. 2000. *Rock mechanics tests of the church of Serra do Pilar Monastery*. Technical report. LNEC, Lisbon (in Portuguese)
Page, J. 1993. *Masonry arch bridges. State-of-the-Art Review*. Transport Research Laboratory, Department of Transport. London: HMSO.
Potyondy, D.O. and Cundall, P.A. 2004. A bonded-particle model for rock. *International Journal of Rock Mechanics & Mining Sciences*, n. 41, p. 1329-1364.
Rouxinol, G.A.F., Providência, P. and Lemos, J.V. 2006. The discrete element method with 2D rigid polygonal and circular elements. In P.B. Lourenço, P. Roca, C. Modena and S. Agrawal (eds.), Proc. *V Int. conf. structural analysis of historical constructions*, vol. 2, p. 1023-1030. New Delhi: Macmillan.
Valença, J. 2006. *Photogrammetric techniques in structural engineering*. M.Sc. Thesis, University of Coimbra, Portugal (in Portuguese)
Vermeltfoort, A.T. 2001. Analysis and experiments of masonry arches. In P.B. Lourenço and P. Roca (eds.), *Historical Constructions*, *Proc. 3rd Int. Seminar, p*. 489-498, Guimarães: University of Minho.
Vieira J.L.M. 1997. *A discrete element model for the study of masonry structures*. M.Sc. Thesis, Instituto Superior Técnico, Lisbon (in Portuguese).
Williams, J.R. 1988. Contact analysis of large numbers of interacting bodies using discrete modal methods for simulating material failure on the microscopic scale. *Eng. Computations* 5, p. 198-209.